Published in final edited form as:
J Cell Sci. 2017 February 15; 130(4): 791–804. doi:10.1242/jcs.187914.

Pex35 is a regulator of peroxisome abundance

Ido Yofe[1], **Kareem Soliman**[2], **Silvia G. Chuartzman**[1], **Bruce Morgan**[3,4], **Uri Weill**[1], **Eden Yifrach**[1], **Tobias P. Dick**[4], **Sara J. Cooper**[5], **Christer S. Ejsing**[6], **Maya Schuldiner**[1,*], **Einat Zalckvar**[1,*], **Sven Thoms**[2,*]

[1]Department of Molecular Genetics, Weizmann Institute of Science, Rehovot 7610001, Israel

[2]Department of Child and Adolescent Health, University Medical Center, Göttingen 37075, Germany

[3]Department of Cellular Biochemistry, University of Kaiserslautern, Kaiserslautern 67653, Germany

[4]Division of Redox Regulation, ZMBH-DKFZ Alliance, German Cancer Research Center (DKFZ), Heidelberg 69121, Germany

[5]HudsonAlpha Institute for Biotechnology, Huntsville, AL 35806, USA

[6]Department of Biochemistry and Molecular Biology, VILLUM Center for Bioanalytical Sciences, University of Southern Denmark, Odense 5230, Denmark

Abstract

Peroxisomes are cellular organelles with vital functions in lipid, amino acid and redox metabolism. The cellular formation and dynamics of peroxisomes are governed by *PEX* genes; however, the regulation of peroxisome abundance is still poorly understood. Here, we use a high-content microscopy screen in *Saccharomyces cerevisiae* to identify new regulators of peroxisome size and abundance. Our screen led to the identification of a previously uncharacterized gene, which we term *PEX35*, which affects peroxisome abundance. *PEX35* encodes a peroxisomal membrane protein, a remote homolog to several curvature-generating human proteins. We systematically characterized the genetic and physical interactome as well as the metabolome of mutants in *PEX35*, and we found that Pex35 functionally interacts with the vesicle-budding-inducer Arf1. Our results highlight the functional interaction between peroxisomes and the secretory pathway.

*Authors for correspondence (maya.schuldiner@weizmann.ac.il; einat.zalckvar@weizmann.ac.il; sven.thoms@med.uni-goettingen.de).

Competing interests
The authors declare no competing or financial interests.

Author contributions
M.S. and S.T. conceived the study. I.Y., T.P.D., C.S.E., M.S., E.Z. and S.T. conceived and supervised the experiments. I.Y. performed the majority of the experiments in this manuscript. S. Chuartzman performed the high content screen. K.S. performed the STED experiments and the oleate growth assays. B.M. and T.P.D. measured the redox status of peroxisomes. C.J.E. performed the lipidomics analysis. S.T. performed peroxisome purification. S. Cooper, K.S. and S.T. conducted amino acid analyses. All authors analyzed the data. I.Y., M.S., E.Z. and S.T. wrote the manuscript.

Europe PMC Funders Author Manuscripts

Keywords

Peroxisomes; Pex35; Ygr168c; Arf1; High-content screen; Yeast

Introduction

Of the cellular organelles, peroxisomes are among the most poorly understood. Peroxisomes are equipped with only a modest number of proteins (~100) and have a diameter in the range of the resolution of light microscopes (~200 nm) but they are extremely dynamic in size, number and protein content (Smith and Aitchison, 2013). In addition, peroxisomes are intriguing and central organelles due to their involvement in various cellular metabolic pathways, such as those of lipids, reactive oxygen species (ROS), carbohydrates, polyamines and amino acids (Wanders and Waterham, 2006), as well as their contribution to an increasing number of non-metabolic functions, such as innate immunity (Dixit et al., 2010; Magalhães et al., 2016; Odendall et al., 2014).

It is not surprising therefore that malfunction of peroxisomes leads to peroxisome-specific diseases (Braverman et al., 2013; Weller et al., 2003) and contributes to the pathology of Alzheimer's and Parkinson's diseases, aging, cancer, type 2 diabetes and heart failure (Beach et al., 2012; Colasante et al., 2015; Fransen et al., 2013; Islinger et al., 2012; Trompier et al., 2014). A useful distinction divides peroxisomal diseases into two groups: those in which single enzymatic functions are defective, and those where peroxisome biogenesis is defective per se. In peroxisome biogenesis disorders (PBD), genes involved in peroxisome formation or maintenance are mutated. Such genes are termed *PEX* genes, and the proteins they encode are termed peroxins. In humans, 16 *PEX* genes are known (Thoms and Gärtner, 2012; Wanders and Waterham, 2006). Nearly all of the human *PEX* genes have orthologs in yeasts; however, yeasts have additional *PEX* genes without obvious homologues in mammals. *PEX34* from the yeast *Saccharomyces cerevisiae*, a recent addition to the growing list of *PEX* genes, encodes a peroxisomal membrane protein that functions together with the Pex11 family to control peroxisome number (Tower et al., 2011). The Pex11 family in yeast encompasses the orthologous proteins Pex11, Pex25 and Pex27, and is involved in peroxisome division and proliferation (Thoms and Erdmann, 2005). Therefore, the Pex11 family is also referred to as PEX11-type of peroxisome proliferators (PPP) (Kettelhut and Thoms, 2014; Thoms and Gårtner, 2012). Despite the identification of new genes involved in division and proliferation our understanding of peroxisome division is still partial, and hence in-depth characterization of the functions of known effectors as well as discovery of more players in this process is forthcoming.

Classically, *PEX* genes have been identified by complementation screens using mammalian cells or yeast cells (Just and Kunau, 2014). The earlier yeast screens for *PEX* genes were based on the finding that β-oxidation in yeast is exclusively located in the peroxisome so that only peroxisome-competent cells were supposed to be able to utilize oleic acid as a sole carbon source (Just and Kunau, 2014). More recently, it was shown that oleic acid becomes toxic when some peroxisomal functions are compromised (Lockshon et al., 2007) and genes with these functions can therefore not be identified in traditional screen settings. Also, owing

Europe PMC Funders Author Manuscripts

to the experimental limitations inherent in classical forward genetic screens, yeast screens for peroxisomal functions have identified mainly non-essential genes with strong phenotypes. Other, *non-PEX* genes that are required for peroxisome biogenesis or function have been identified by more dedicated approaches. These include the Sec61 ER translocon complex as an entry point into the endomembrane system for peroxisomal membrane proteins (Thoms et al., 2011a); or the ADP-ribosylation factors (ARFs), small GTPases involved in the control of many vesicular processes, that are also required for peroxisome formation (Anthonio et al., 2009; Lay et al., 2006).

So how can we identify more proteins required for peroxisomal function? In recent years this has been achieved by both genome-wide screens and dedicated proteomic analyses. For example, proteomics screens of peroxisomes were able to identify new peroxisomal proteins in fungi (Marelli et al., 2004; Schäfer et al., 2001; Thoms et al., 2008; Yi et al., 2002), plants (Eubel et al., 2008; Fukao et al., 2002; Reumann et al., 2007, 2009) and mammalian tissues, such as rat liver (Islinger et al., 2007, 2010; Kikuchi et al., 2004), mouse liver and kidney (Mi et al., 2007; Ofman et al., 2006; Wiese et al., 2007), and human liver (Gronemeyer et al., 2013). In addition, several genome-wide genetic screens in yeast have shed light on new proteins and their potential functions. For example, fitness and transcriptome responses to oleic and myristic acid have been used to define the networks underlying the metabolic responses to these fatty acids and to identify new proteins involved in peroxisome function (Lockshon et al., 2007; Smith et al., 2002, 2006). A collection of kinase and phosphatase gene deletion strains has also been evaluated for the expression of the peroxisomal matrix protein enzyme 3-ketoacyl-CoA thiolase (Pot1) (Saleem et al., 2008). Following a similar approach, a genome-wide screen for alterations in the expression of a GFP-labeled peroxisomal matrix protein led to the identification of 169 genes required for all the processes that lead to faithful biogenesis and propagation of peroxisomes (Saleem et al., 2010). Other systematic approaches including high-throughput experiments with quantitative analysis and modeling have been used to complete the peroxisomal proteome and to improve the understanding of peroxisome metabolism and biogenesis (Cohen et al., 2014; Wolinski et al., 2009). More recently, systematic high-content screens and bioinformatics analyses led to the identification of a new peroxisomal targeting protein, Pex9, and two new peroxisome matrix proteins, Pxp1 and Pxp2 (Effelsberg et al., 2016; Nötzel et al., 2016; Yifrach et al., 2016; Yofe et al., 2016). With each new study revealing additional new peroxisomal proteins it is clear that we have not yet saturated our understanding of the peroxisomal proteome and new peroxisomal proteins await discovery.

In this work, we report the results of a high-content screen in the yeast *Saccharomyces cerevisiae*, tailored to uncover mutants affecting peroxisome abundance. By creating a systematic library of gene mutants in yeast cells expressing a fluorescent marker for peroxisomes, followed by automated microscopy and computational image analysis, we identified a previously uncharacterized protein affecting peroxisome abundance. We show that this protein, which we name Pex35, is a peroxisomal membrane protein that controls peroxisome abundance.

Results

A high-content screen uncovers regulators of peroxisome size and number

In order to identify genes that regulate peroxisome number or size, we wanted to quantify these parameters in mutants of every yeast gene. To this end we created a query strain that enables visualization of peroxisomes and is compatible with the Synthetic Genetic Array (SGA) automated mating approach in yeast (Cohen and Schuldiner, 2011; Tong and Boone, 2006). The strain expressed the peroxisomal membrane protein Pex3 tagged with the red fluorescent protein mCherry (Pex3-mCherry), and a fluorescent marker for the endoplasmic reticulum (ER), Spf1-GFP, to enable automated cell segmentation. The query strain was then crossed into nearly 5000 strains of the deletion library (Giaever et al., 2002) and more than 1000 strains of the DAmP (Decreased Abundance by mRNA Perturbation) hypomorphic allele library for essential genes (Breslow et al., 2008). Following sporulation and selection of haploids, we obtained about 6000 unique haploid strains, each mutated in one yeast gene and marked with Pex3-mCherry and Spf1-GFP. This screening library was subjected to automated image acquisition and analysis during growth in glucose. Using an automated high-content microscopy setup specifically configured for this purpose (Breker et al., 2013), we recorded three images covering hundreds of cells per strain (Fig. 1A). We then developed a computational pipeline using the green fluorescent ER marker to find individual cells and counted the mean size of peroxisomes as well as their number per cell (Fig. S1). When analyzing peroxisome size (Fig. 1B; for complete data see Table S1) we found that mean cell peroxisome size varied through a range of approximately sixfold. Although some peroxisomal proteins and proteins associated with peroxisome formation were enriched at the edges of the distribution, there was no strong enrichment or near-complete coverage of mutants in peroxisomal proteins or peroxisome biogenesis factors in the strains with decreased or increased peroxisome size. Rather, genes controlling mitochondrial function or localization were dramatically enriched. Among the top 130 mutants with enlarged peroxisomes, 80 were mitochondrial proteins (five-fold enrichment, P-value=2×10^{-31}) (Eden et al., 2009), confirming a tight connection between peroxisomes and mitochondria (Cohen et al., 2014; Mohanty and McBride, 2013; Schrader et al., 2013; Thoms et al., 2009). Indeed it is known that when mitochondrial metabolism is compromised, cells can compensate by upregulating peroxisome metabolism and size (Eisenberg-Bord and Schuldiner, 2016). Interestingly, a mutant causing some of the smallest peroxisomes was defective in carbamoyl phosphate synthase (Cpa1), which is important for the biosynthesis of the amino acid citrulline. These findings indicate that peroxisome size is not the best parameter to identify new peroxisomal proteins. However, the information regarding size may be used in the future to further understand the factors that create the functional link between mitochondria and peroxisomes.

When focusing on peroxisome number, we noticed that mutants with increased peroxisome number were not enriched for peroxisomal proteins and seemed to have defects in central cellular processes like translation, chromatin control or cytoskeletal dynamics (Fig. 1C; Table S1). However, the strains with the strongest reduction in peroxisome number were strikingly enriched in known peroxisomal membrane proteins (105-fold enrichment, P-value=10^{-26}) (Eden et al., 2009) (Fig. 1C). Among those are strains known to affect

peroxisome morphology (*Δpex19, Δpex27, Δinp1* and *Δvps1*). At the other end of the spectrum, loss of Pex17, a protein that is associated with the docking complex for peroxisome matrix protein import (Huhse et al., 1998), caused a drastic increase in peroxisome number. Importantly, several unknown proteins affected peroxisome number to a similar extent as mutations in known peroxisomal proteins [Fig. 1C (inset) and Table 1]. Of those, the most highly ranking uncharacterized open reading frame was *YGR168C*.

Deletion or overexpression of *YGR168C* affects peroxisome number and function

We decided to focus on *YGR168C* since a deletion of this previously uncharacterized gene caused a decrease in peroxisome abundance that is as dramatic as defects in the known peroxisomal biogenesis and inheritance proteins Pex12 and Vps1 (Fig. 2A). To ensure that this phenotype is independent of the peroxisomal marker (Pex3-mCherry) that we chose for the initial screen, we deleted *YGR168C* in four strains with GFP-tagged peroxisomal markers, including both matrix and membrane proteins. We found that peroxisome recognition of our image analysis program depended on the intensity of the marker used and the analysis settings. Therefore, peroxisome abundance values from measurement of fluorescent markers should be stated in arbitrary units that may only be used to compare between strains with the same marker. However, regardless of the marker used, loss of *YGR168C* caused a significant reduction in peroxisome number per cell when compared to a control strain (Fig. 2B).

Next, we manipulated Ygr168c protein expression by putting it under control of the strong *TEF1* promoter ($TEF1_{prom}$). Overexpression of *YGR168C* also led to a decrease in peroxisomal fluorescent puncta either in glucose (Fig. 2C) or oleic acid as a sole carbon source (Fig. 2D). The fact that both deletion and overexpression caused similar phenotypes was puzzling to us and we decided to follow peroxisomal architecture in more detail.

Super-resolution microscopy demonstrates that *YGR168C* overexpression leads to multi-lobular peroxisome morphology

To better characterize the effect on peroxisomes produced by either deletion or overexpression of *YGR168C* we analyzed peroxisome size and morphology by stimulated emission depletion (STED) microscopy. Strains were transformed with a plasmid expressing a peroxisome-targeted GFP variant (EYFP-SKL) and were analyzed by fluorescence nanoscopy using nanobodies directed against GFP.

First, using STED microscopy we determined the size of peroxisomes with unprecedented accuracy. We used images of 71 peroxisomes to determine that the diameter of wild-type peroxisomes is 174 nm (±8 nm, s.e.m.), which is below the resolution of conventional light microscopy (Fig. 3A,D; Fig. S2A). Second, these images, as opposed to regular diffraction-limited analysis, revealed a clue as to the basis of the function of *YGR168C*. While the number of peroxisomes was reduced in *Δygr168c*, their size was not (Fig. 3B,D; Fig. S2A). However, peroxisomes in the overexpressing strain, which appeared to be enlarged in confocal microscopy analysis, showed a striking multi-lobular morphology when analyzed by STED microscopy (Fig. 3C,D; Fig. S2A). This phenotype may be due to hyper-fission of the organelles into tiny peroxisomes, which clump together giving the false impression of a

single big peroxisome when visualizing cells by fluorescence microscopy; alternatively the multi-lobular phenotype may be due to the initiation of a proliferation process that is aborted at an early stage. Both scenarios are compatible with a role of Ygr168c in controlling peroxisome fission. Loss of *YGR168C* may therefore cause the opposite effect – reduction in fission – causing the observed reduction in peroxisome number. Taken together our results demonstrate that Ygr168c is a bona fide regulator of peroxisome number and size in yeast.

YGR168C is a new *PEX* gene, which we denote *PEX35*

Since Ygr168c has such a strong effect on peroxisome number and size, we wanted to better characterize this protein. The C-terminally tagged strain could not be visualized above background autofluorescence when expressed under its own promoter in cells growing in glucose medium, indicating that expression of the protein in glucose medium is very low. When we expressed the protein with either a C- or N-terminal fluorescent tag under control of the medium strength *TEF1* promoter, Ygr168c tagged on either terminus was localized to punctate structures that completely colocalized with the peroxisomal markers Pex3-mCherry or Pex3-GFP (Fig. 4A). The Ygr168c protein is predicted by TMHMM (Krogh et al., 2001) and TOPCONS (Bernsel et al., 2008) to be a membrane protein with five transmembrane domains and a large C-terminal domain facing the cytosol (Fig. 4B). We examined the expression and localization of GFP-Ygr168c in the absence of Pex19, a farnesylated membrane protein biogenesis factor (Rucktåschel et al., 2009). In *Δpex19* cells, the residual GFP signal is distributed in the cytosol and the ER (Fig. 4C). These findings further support that Ygr168c is a peroxisomal protein that is withheld in or mislocalized to the ER in the absence of Pex19. Similar results were obtained in the absence of PEX3. GFP-Ygr168c expression was reduced and the residual GFP signal was distributed in the cytosol and the ER (Fig. S2B), in agreement with Ygr168c being a peroxisomal protein. To confirm that Ygr168c is a bona fide peroxisomal protein, we purified peroxisomes from oleate-induced wild-type cells with a GFP-marked Ygr168c. Ygr168c was recovered from the peroxisome fraction of the Nycodenz density gradient (24%-35% interface) and was absent in the cytosolic and the mitochondrial fractions (Fig. 4D).

The N-terminal domain of Ygr168c is predicted to contain a mitochondrial-targeting signal (MTS) (Emanuelsson et al., 2007). As some peroxisomal membrane proteins can be dually targeted to mitochondria, we analyzed the intracellular localization of an N-terminal fragment of Ygr168c comprising the first and second predicted transmembrane domain (TMD; amino acids 1 to 107) that contain the predicted MTS as a fusion protein with mCherry. Mitochondrial targeting of the truncated protein was not observed, suggesting that the N-terminal domain does not function as an MTS in this context or under these conditions. Interestingly, this fusion protein now localized to both the ER and peroxisomes (Fig. 4E), in agreement with the proposed passage of peroxisomal membrane proteins through the ER (van der Zand et al., 2010). Our finding also suggests that peroxisome-specific targeting information is in the C-terminal domain of Ygr168c.

The hallmark of many strains with a defect in maintaining normal peroxisome abundance is a growth defect when grown on oleic acid as the sole carbon source. Indeed, the deletion of *YGR168C* did not affect growth on glucose (Fig. S2C), yet showed reduced growth and

reduced formation of halos on oleic acid medium, demonstrating the lack of oleic acid consumption (Fig. S2D). Interestingly, the overexpression did not give a similar phenotype (Fig. S2E). However, overexpression of a GFP-tagged isoform *(TEF1$_{prom}$:GFP-YGR168C)* did cause a phenotype suggesting that it somehow aggravates the effect of overexpression or creates a dominant negative (Fig. S2E). Growth curves of these strains on oleate as a sole carbon source confirm this finding: the growth of *Δygr168* and *TEF1$_{prom}$:GFP-YGR168C* is slower than a control strain although is better than *Δpex3* (Fig. 4F). Quantitative assessment of oleate consumption at the end point of the growth assay showed that mutant cells indeed utilized less of the available oleic acid (Fig. 4G).

Finally, we assayed the accumulation of peroxisomes in real time. The *GAL1* promoter was introduced to regulate GFP-Ygr168c in a strain containing Pex3-RFP as a peroxisomal marker. Time-lapse microscopy following a transfer of this strain from glucose- to galactose-containing medium showed that GFP-Ygr168c accumulated in Pex3-marked peroxisomes. Furthermore, while cells that did not show GFP-Ygr168c expression had a normal peroxisome abundance, cells with GFP-Ygr168c expression displayed an abnormal phenotype of one enlarged peroxisome per cell over time (Fig. 4H).

Taken together, these data show that Ygr168c is a new peroxisomal membrane protein in yeast. Manipulation of the expression level of Ygr168c led to changes in peroxisome number and size, as well as to growth defects on oleate. As Ygr168c bears all signs of a peroxin, we named it Pex35.

Characterizing the molecular function of Pex35

Having identified a new peroxisomal membrane protein, we were eager to functionally characterize it and understand how it exerts its effect on peroxisome number and size. Since peroxisomes have an important role in lipid metabolism, we first performed a detailed lipidomic analysis but could find no significant changes in wholecell lipid composition compared to a control strain (Table S2). This result suggests that Pex35 does not influence gross membrane lipid composition. Coupled with the relatively small growth defect of *Δpex35* strains grown on oleic acid our results suggest that Pex35 is not directly involved in lipid metabolism.

We then performed a synthetic growth screen to try and uncover proteins or pathways that become important when cells are lacking Pex35. In this screen, a *Δpex35* strain was crossed with the libraries comprising the ~6000 deletion and hypomorphic strains that we had previously used for the visual screen. After mating, sporulation and selection of haploids, growth of the double mutants was compared to growth of the individual mutant strain (Table 2; Table S3). Focusing on synthetic lethal interactions where the double mutants are dead while each single mutant is alive, we saw that redox homeostasis becomes important in the absence of Pex35. For example, deletion of the glutathione (GSH) synthetase *(GSH2)* required for the synthesis of GSH from γ-glutamyl cysteine and glycine was synthetic lethal with *Δpex35*. This suggests that the mutant strongly depends on a reducing environment for survival. To test this, we measured the glutathione redox potential in the peroxisomal matrix using a newly described peroxisomal reporter (Elbaz-Alon et al., 2014). Notably, overexpression of Pex35 had already caused a substantial pro-oxidative shift under steady

state conditions. Moreover, following treatment with a bolus of hydrogen peroxide, the probe remained more reduced in the deletion strain whereas it became more oxidized upon overexpression of Pex35 (Fig. S2F).

Other pathways that were over-represented were those of polyamine, cysteine, lysine and arginine biosynthesis (Table 2). To test how amino acid levels are altered in the absence of Pex35, we extracted metabolites from wild-type, *Δpex35, TEF_{prom}: GFP-PEX35* and *Δpex3* strains. We used high-performance liquid chromatography (HPLC)-based metabolomics to characterize amino acid levels in each strain and found that amino acid levels were indeed significantly affected (Fig. S2G). There was a remarkable 70% reduction in the level of citrulline in *Δpex35*, which was matched by a more than two-fold increase of citrulline in *TEF_{prom}:GFP-PEX35*. This was in agreement with the strong lethality of this strain in combination with mutants in the arginine biosynthetic pathway. These findings reinforce the notion that peroxisomes in yeast are important in regulating or executing aspects of amino acid metabolism (Natarajan et al., 2001), and highlights how defects in mitochondrial function (such as in arginine biosynthesis) can activate the retrograde response to enhance peroxisomal functions (Chelstowska and Butow, 1995).

Pex35 is located in the proximity of Pex11 family proteins and Arfs

So far, our data suggested that Pex35 is a peroxisome membrane protein affecting peroxisome number and size, as well as redox and amino acid homeostasis. To try and understand the mechanism by which Pex35 functions, we performed a systematic complementation assay using the two parts of a specially adapted dihydrofolate reductase (DHFR) enzyme (Tarassov et al., 2008). In this assay, one half of the DHFR enzyme is fused to Pex35 (‘bait’), which is expressed in ~5700 yeast strains expressing fusions of each individual proteins with the other half of DHFR (‘prey’). When the Pex35 bait is in proximity to one of the library prey proteins, methotrexate-resistant DHFR activity is reconstituted, and cells can grow in the presence of methotrexate, an inhibitor of the endogenous essential DHFR activity (Fig. 5A).

When seeking for growth with an N-terminally tagged Pex35, we could not find any high-confidence complementing proteins, suggesting that the N-terminus is essential for the interaction of Pex35 with effector proteins localized at the peroxisome (data not shown) and reinforcing the previous notion that the overexpression of an N-terminally tagged GFP-Pex35 is more toxic than regular overexpression. However, when we performed the assay with a C-terminally tagged strain, either under the native Pex35 promoter or the strong *TEF1* promoter, we identified 11 proteins previously known to be involved in peroxisomal functions among the top 16 hits (Fig. 5B,C; Table S4). These included Pex19, the peroxisomal membrane protein chaperone, supporting the notion that Pex35 is a membrane protein. Other proteins that were in the vicinity of Pex35 were peroxisomal membrane proteins or membrane-associated proteins (enrichment factor 70, $P=1.6\times10^{-17}$) (Eden et al., 2009). Especially intriguing was the identification of the Pex11 family proteins, Pex11 and Pex25, and Arf1, because these proteins have previously been shown to interact with each other, and all of them have a role in peroxisome fission, a process that would affect peroxisome number and size (Fig. 5B,C).

Europe PMC Funders Author Manuscripts

Pex35 modulates the effect of Arf1

To examine whether the physical proximity with Arf1 can explain the effect of Pex35 on peroxisome abundance, we first tested whether the abundance of Arf1 or the localization of Arf1–mCherry were affected by deleting or overexpressing Pex35. We found that both deletion and overexpression of *PEX35* dramatically increased Arf1 levels (Fig. S3A). Moreover, *PEX35* also affected Arf1-mCherry distribution. In control strains, Arf1 localizes mainly in punctate structures, in agreement with the Golgi localization of Arf1 (Stearns et al., 1990). However, when *PEX35* was deleted or the tagged form was overexpressed, Arf1 redistributed to various internal membranes (Fig. 6A). It is well known that, while the C-terminal tag of Arf1 creates a dysfunctional form, it does report accurately on its subcellular localization (Huh et al., 2003; Jian et al., 2010).

Arf1 has previously been implicated in peroxisome formation (Anthonio et al., 2009; Lay et al., 2005; Passreiter et al., 1998). We therefore investigated whether Pex35 was mediating its effect on peroxisome abundance through Arf1 by looking at the effect of *Δpex35* deletion or overexpression on the background of loss of Arf1 (Δarf1). Deletion of *ARF1* in the *Δpex35* knockout lead to a marked increase in peroxisome size and aggravated the effect of Δ*pex35* on peroxisome number (Fig. 6B,C). Even more striking, the deletion of *ARF1* in the Pex35-overexpressing strain rescued the peroxisome-enlarging effect of Pex35 overexpression and normalized the number of peroxisomes to control levels (Fig. 6B,C). These findings suggest that Pex35 exerts its function through a mechanism that requires Arf1.

Next, we wanted to analyze Arf1 at the organellar level. We purified peroxisomes by cell fractionation from strains that contained both GFP-tagged Pex3 as a peroxisome marker and RFP-tagged Arf1, either in a wild-type or in a Δ*pex35* background (Fig. S3B). The absence of the peroxisome marker in the cytosol or the mitochondria fraction showed that other compartments were free from peroxisomes. Arf1–RFP was clearly enriched in the peroxisome and mitochondria fractions, in agreement with the results of the quantitative whole-cell analysis (Fig. S3A). The distinction of peroxisomal and mitochondrial pools of Arf1, however, was not possible in this experiment, because the ‘light-mitochondrial’ faction co-fractionates with peroxisomes in the step gradient.

Our findings on the effects of Pex35 on Arf1 made us wonder whether altering *PEX35* could exert an effect on the secretory pathway functions of Arf1 (Fig. 6A). In order to test whether Arf1-dependent anterograde traffic was affected, we tested secretion of the intra-ER chaperone Kar2 (a BiP homolog). The slow leak of Kar2 from the ER, through the Golgi and its secretion into the medium is a good way to observe dysregulated secretion (Copic et al., 2009). Indeed, overexpressing GFP-Pex35 (which led to a drastic increase in Arf1 levels) decreased secretion to 50% or less, similar to what is seen upon directly overexpressing Arf1 (Fig. 6D). Interestingly, the deletion of *PEX35* (although also leading to Arf1 overexpression) could compensate for the effect of Arf1 overexpression, suggesting that in normal physiology *PEX35* restrains Arf1 function (Fig. 6D). Equally striking was the finding that the deletion of *PEX3* alone exerted a secretion defect in the same range, like strong activation of the unfolded protein response (UPR; seen by deletion of the ER protein *SPF1)*, or the overexpression of Pex35 or Arf1 (Fig. 6D). To follow up this finding, we tested the localization of Arf1-RFP in a *Δpex3* background. The deletion of *PEX3* led to a

surprising loss of focal Arf1 localization (Fig. 6E). At this point it is not clear whether this is due to a direct association of Arf1 with Pex3 or Pex35, or if it is due to the upregulation of Arf1 or the large proportion of Arf1 associated with peroxisomes that is altered upon Pex3 loss, but in all these cases, these data point to a strong role for peroxisomes in the function of the secretory pathway.

Discussion

One of the current challenges in molecular cell biology is to integrate multiple levels of understanding spanning holistic omics approaches and detailed analysis of single molecular entities. In this study, we go through such an analysis, starting from a large-scale genetic screen with the complete deletion and DAmP collection, and end up with the identification of a new peroxisomal protein and insights into the mechanism by which it may regulate peroxisome abundance.

The initial screen relied on three automated stages: generation of a screening library comprising deletions and functional knockdowns of nearly all yeast genes, automated image acquisition, and a computational pipeline for image segregation and quantification. This approach complements the classical forward genetic screen based on growth on oleate, with the advantage of increased sensitivity gained by statistical analysis of quantitative data. Our screen was stringent as well as exhaustive – most other genes previously implicated in many aspects of peroxisome formation, inheritance and maintenance clustered on the top of our scoring list. We found that, although some strains defective in peroxisome proliferation have a strongly altered (reduced) peroxisome size, reduction in peroxisome number is a more exhaustive criterion to cover genes required for peroxisome formation and maintenance.

Of the genes with the strongest effect on peroxisome number, we decided to focus on *YGR168C*, which we termed *PEX35*. We show that Pex35 is a peroxisomal membrane protein that had not been identified previously, probably due to its low expression level in cells grown on glucose and its moderate, yet quantifiable, effect on peroxisome number and size. Deletion of *PEX35* leads to a reduction in peroxisome number, and overexpression of *PEX35* to an increase in hyper-fissioned aggregated tiny peroxisomes or to an early block in the proliferation of peroxisomes. These results, together with the oleate growth phenotypes, classify Pex35 as a bona fide peroxin.

We found that C-terminally tagged Pex35 localizes in the vicinity of the Pex11-type of peroxisome proliferators Pex11, Pex25 and Pex34, and the small GTPase Arf1. All of these proteins are known to influence peroxisome abundance (Lay et al., 2006; Thoms and Erdmann, 2005; Tower et al., 2011), so it is attractive to speculate the Pex35 is part of a regulatory unit that controls peroxisome fission, and therefore numbers, in the cell. The effect on Arf1 was particularly intriguing, because ARFs have previously been implicated in peroxisome formation, but their contribution has been poorly established. The mammalian ARF proteins Arf1 and Arf6 have been shown to be present on rat liver peroxisomes, and to bind to peroxisomes in a GTP-specific manner. Interference with either Arf1 or Arf6 changes peroxisome morphology (Anthonio et al., 2009; Lay et al., 2005; Passreiter et al., 1998). In yeast, the ARF proteins Arf1 and Arf3 are required for peroxisome fission albeit in

opposing manners (Anthonio et al., 2009; Lay et al., 2005). Additional support of the involvement of ARFs in peroxisome function comes from the finding that the expression of a dominantnegative Arf1 mutant, Arf1Q71L, blocks protein transport from the ER to the peroxisome in plant cells (McCartney et al., 2005). However, whether ARFs are actively recruited to peroxisomes, how ARFs affect peroxisomes and how this affects general cellular trafficking fidelity is still a mystery.

Initially, Pex11 was suggested to be the receptor of ARFs and coatomer on peroxisomes (Passreiter et al., 1998). This notion was questioned when it was found that mutations that prevent coatomer binding to Pex11 had no effect on peroxisome function in yeast or trypanosomes (Maier et al., 2000). In addition, the COPI inhibitor, brefeldin A, does not inhibit peroxisome biogenesis (South et al., 2000; Voorn-Brouwer et al., 2001). However, today there is new evidence for the involvement of membrane coats in peroxisome function (David et al., 2013; Dimitrov et al., 2013; Lay et al., 2006) and it is becoming clear that peroxisome biogenesis may be distinct from peroxisome maintenance by fission. Moreover, as we saw in our own work, fluorescence microscopy alone may not be a sensitive enough readout for such changes, as sub-diffraction images can give more detailed information that may be easier to reconcile with genetic data.

In recent years, reports on non-vesicular functions of ARFs are becoming more common (Jackson and Bouvet, 2014). We found that either deletion or overexpression of Pex35 drives Arf1 out of its physiological localization, mirroring the phenotype of an increased GAP function or a reduced GEF function, because the active GTP-bound form of Arf1 is recruited to the membrane, whereas the inactive GDP-bound form is released from the membrane (Donaldson and Jackson, 2011). Of note, the Arf1-GEF Sec7 was also found in the proximity of Pex35 in our DFHR screen (Table S4, rank 29), although the significance of that interaction remains to be established. While deletion of Pex35 elevates Arf1 protein levels (Fig. S3A), we do not understand its mechanistic connection with Arf1. It may very well be that the upregulation of Arf1 is a consequence of reduced cellular function and cellular compensation mechanisms. In support of this, the ability of overexpression of Arf1 to reduce leakage of Kar2 is abolished in the absence of Pex35 (Fig. 6D).

Our findings illuminate both the role of Arf1 as a regulator of peroxisome abundance and its dependency on healthy peroxisome biogenesis. Pex35 may be the crucial link in these processes: loss of focal localization of Arf1 in a peroxisome-defective *Δpex3* strain may be due to the loss of peroxisomal recruitment of Arf1 in this strain.

Intriguingly, Pex35 has domains that show homology with three human proteins (Fig. S4), two of which have membrane-shaping properties. One region of Pex35 is homologous to human Rtn1, an ER reticulon, and another with Epn4, an epsin-related protein that binds the clathrin coat. Both proteins shape membrane curvature, which is essential for the fission process. In addition, potential homology was also found to Pxmp4, a human peroxisomal protein. These areas of homology suggest that Pex35 functions have been conserved in humans and they are suggestive of possible mechanism of Pex35 function.

Our work suggests that regulation of peroxisome size and number is linked tightly with secretory pathway functions. Physiological secretion is dependent on the presence of peroxisomes. On the other hand, peroxisome formation itself requires a functional secretory pathway. In this way, the metabolic status of the cell could be coupled to secretion and growth in a simple and elegant mechanism. Such a cross-talk between these two systems could have dramatic effects on cellular homeostasis and hence would impact peroxisomes in health and disease.

Materials and Methods

Yeast strains

All yeast strains in this study are based on the BY4741/2 laboratory strains (Brachmann etal., 1998). Strains created in this study are listed in Table S5. All genetic manipulations were performed using the lithium acetate, polyethylene glycol (PEG) and single-stranded DNA (ssDNA) method for transforming yeast strains (Gietz and Woods, 2006) using plasmids previously described (Janke et al., 2004; Longtine et al., 1998), as listed in Table S6. Primers for genetic manipulations and their validation were designed using Primers-4-Yeast (Yofe and Schuldiner, 2014), as listed in Table S7.

A query strain was constructed by introduction of an ER marker, Spf1-GFP, and a peroxisome marker, Pex3-mCherry (yMS1233). The query strain was then crossed into the yeast deletion and hypomorphic allele collections (Breslow et al., 2008; Giaever et al., 2002) by the synthetic genetic array method (Cohen and Schuldiner, 2011; Tong and Boone, 2006). Representative strains of the resulting screening library were validated by inspection for the presence of peroxisomal mCherry and ER-localized GFP expression. This procedure resulted in a collection of haploid strains used for screening mutants that display peroxisomal abnormalities.

Automated high-throughput fluorescence microscopy

The screening collection, containing a total of 5878 strains, was visualized in SD medium during mid-logarithmic growth using an automated microscopy setup as described previously (Breker et al., 2013).

Automated image analysis

After acquisition, images were analyzed using the ScanR analysis software (Olympus), by which single cells were recognized based on the GFP signal, and peroxisomes were recognized based on the mCherry signal (Fig. S1). Measures of cell and peroxisome size, shape and fluorescent signals were extracted, and outliers were removed. A total of 5036 mutant strains were successfully analyzed, with a mean of 126±56 (s.e.m.) cells per strain (minimum of 30) that passed filtering (Table S1). For each mutant strain, the mean number of peroxisomes recognized by the software per cell was extracted, as well as the mean area (in pixels) of peroxisomes. Note that these are arbitrary units that may only be used to compare between strains, as resulting values are dependent on the parameters of image analysis and of the fluorescent markers used.

Microscopy

For follow up microscopy analysis, yeast growth conditions were as described above for the high-content screening. Imaging was performed using the VisiScope Confocal Cell Explorer system, composed of a Zeiss Yokogawa spinning disk scanning unit (CSU-W1) coupled with an inverted Olympus microscope (IX83; ×60 oil objective; excitation wavelength of 488 nm for GFP, and 561 nm for mCherry). Images were taken by a connected PCO-Edge sCMOS camera, controlled by VisView software. In the case of galactose induction of *GALp-GFP-PEX35* (Fig. 3F), yeast were transferred to the microscopy plate, and after adhering to the glass bottom, medium containing 2% galactose was used to wash the cells and during the time-lapse imaging.

STED microscopy

Strains were transformed with EYFP-SKL (plasmid PST1219) and analyzed as described previously (Kaplan and Ewers, 2015) using GFP nanobodies coupled to Atto647N (gba647n-100, Chromotek, Planegg-Martinsried). Slides were analyzed on a custom-made STED setup described previously (Göttfert et al., 2013). Images show unprocessed raw data. STED images shown in Fig. 3 were rescaled by a factor of two using bicubic interpolation (Adobe Photoshop). The size of yeast peroxisomes was calculated as follows. Random peroxisomes were marked by manually drawing a ROI and the center of masses was determined. Peroxisome diameter was measured after drawing a line scan through the minor axis of the peroxisome. The full-width at half-maximum (FWHM) of the Gaussian fits for each peroxisomal structure was determined using an ImageJ macro by John Lim. Average size was quantified for more than 50 peroxisomes and statistical significance was calculated using a two-sample *t*-test (two-tailed, unequal variance).

Oleic acid growth experiments

Growth on oleate, oleate consumption and halo formation was analyzed as described previously (Nötzel et al., 2016; Rucktäschel et al., 2009; Thoms et al., 2008).

Isolation of peroxisomes and mitochondria

Preparation of peroxisomes and mitochondria followed published protocols (Flis et al., 2015; Thoms et al., 2011b). Briefly, yeast cells were grown in YPD (1% yeast extract, 2% peptone, 2% glucose) to late exponential phase, transferred to YPO medium and grown for 48 h. Cells were harvested by centrifugation (3000 ***g*** for 5 min), washed with water and resuspended in buffer containing 0.1 M Tris-HCl, pH 9.4 and 1.5 mg/ml dithiothreitol (DTT). Spheroblasts were prepared by using 2 mg Zymolyase 20 T per 1 g wet weight. Spheroblasts were recovered by centrifugation (3000 **g** for 10 min), washed twice with 1.2 M sorbitol, homogenized and lysed on ice using a Dounce homogenizer in breaking buffer [5 mM 2-(N-morpholino) ethanesulfonic acid (MES), 1 mM potassium chloride, 0.6 M sorbitol, 0.5 mM EDTA, 1 mM phenylmethanesulfonylfluoride (PMSF), pH 6.0 (with KOH)]. Cell debris and nuclei were removed by centrifugation at 3000 **g** for 5 min. The resulting pellet was collected and subjected to two further rounds of resuspension in breaking buffer, homogenizing and centrifugation. The combined (post nuclear) supernatants (PNS) were centrifuged at 20,000 **g** in an SS34 rotor (Sorvall) for 30 min. The organelle

pellets containing peroxisomes and mitochondria were collected and gently resuspended in a small Dounce homogenizer in breaking buffer plus 1 mM PMSF and centrifuged at low speed (3000 **g**) for 5 min to remove residual cellular debris. The supernatant containing the microsomal fraction was centrifuged at 27,000 **g** for 10 min. The pellet was resuspended in breaking buffer and loaded onto a Nycodenz step gradient [steps of 17%, 24%, 35% (w/v) in 5 mM MES, 1 mM potassium chloride, and 0.24 M sucrose, pH 6.0 (with KOH)]. Centrifugation was carried out in a swing out rotor (Sorvall AH-629) at 26,000 rpm for 90 min. Using a syringe, the mitochondrial and the peroxisomal fraction were collected from the top of the 17% and the 24%–35% interface, respectively. Purified organelles were diluted in four volumes of breaking buffer and centrifuged for 15 min at 27,000 **g** in an SS34 rotor. Pellets were stored at —20°C before determination of protein concentration and western blot analysis. Anti-Por1 rabbit antiserum (courtesy of Günther Daum, Institut für Biochemie, Technische Universität Graz, Austria) was used at a dilution of 1:2000 to detect mitochondria.

Arf1 protein quantification

Yeast strains used for protein extraction (BY4741 as wild-type, $GPD1_{prom}$-*PEX35*::natNT2 and Δpex35::natNT2) were grown in YPD (with clonat for Pex35 strains) to the stationary phase and the diluted in YPD to an optical density at 600 nm (OD_{600}) of 0.2 and further grown until they reached an OD_{600} of 0.6-0.8. 2.5 OD_{600} units of yeast cells were harvested by centrifugation (3000 **g** for 3 min). Cells were resuspended in 100 µl distilled water, 100 µl 0.2 M NaOH was added, and cells were incubated for 5 min at room temperature, pelleted (3000 **g** for 3 min), resuspended in 75 µl SDS sample buffer (0.06 M Tris-HCl pH 6.8, 10% glycerol, 2% SDS, 50 mM DTT, 2 mM PMSF and 0.0025% Bromophenol Blue), boiled for 5 min at 95°C and pelleted again (20,000 **g** for 2 min). 25 µl supernatant was loaded per lane for SDS-PAGE (12% acrylamide) and then transferred to a nitrocellulose membrane for western blotting. Primary antibody was rabbit anti-Arf1 (1:2000 dilution, a gift from Chris Fromme, The Weill Institute for Cell and Molecular Biology, Cornell University, Ithaca, USA) and secondary antibody was horseradish peroxidase (HRP)-conjugated anti-rabbit-IgG. Membranes were exposed in LAS4000 machine using chemiluminescence reagents. Quantification was performed by ImageJ relative to a histone H3 loading control.

Protein secretion assay

We analyzed protein secretion as previously described (Copic et al., 2009). Specifically, yeast strains grown in a 96-colony array format were pinned by the RoToR colony arrayer onto YEPD agar plates, and a nitrocellulose membrane was applied onto the plate immediately thereafter. Overnight incubation at 30°C allowed cell growth and ensured that secreted proteins were transferred to the nitrocellulose membrane. The membrane was removed from the plate and then washed (10 mM Tris-HCl, 0.5 M NaCl, pH 7.5) to release remaining cells. Secreted Kar2 was used as a reporter for secretion level, and was probed with a primary rabbit antibody (rabbit polyclonal antiserum, 1:5000 dilution, kindly shared by Peter Walter, Department of Biochemistry and Biophysics, UCSF, San Francisco, USA). Next, we used secondary goat anti-rabbit-IgG conjugated to IRDye800 (926-32211, LI-COR Biosciences) and scanned the membrane for infrared signal using the Odyssey Imaging System (LI-COR Biosciences).

Lipidomics

Quantitative lipid analysis was performed using a Triversa NanoMate ion source (Advion Biosciences, Inc.) coupled to a LTQ Orbitrap XL mass spectrometer (Thermo Fisher Scientific), as previously described (Ejsing et al., 2009).

Glutathione measurements

The thiol-disulfide pair of roGFP2 equilibrates with the glutathione redox couple. roGFP2 exhibits two fluorescence excitation maxima at ~400 nm and ~480 nm for fluorescence emission is followed at 510 nm. The relative intensity of fluorescence emission at each excitation maxima changes in the opposing direction dependent upon whether the roGFP2 thiols are reduced or forming a disulfide bond, thereby allowing ratiometric fluorescence imaging of the roGFP2 redox state. Dynamic E_{GSH} measurements were conducted as previously described in detail (Morgan et al., 2011).

Amino acid analysis

Amino acid analysis was conducted as described previously (Nötzel et al., 2016).

Protein complementation assay screening

The protein-protein interaction screen was performed using the yeast DHFR PCA library as previously described (Tarassov et al., 2008). In brief, strains with Pex35 tagged at its C-terminus with DHFR[1,2] (in MATa), or DHFR[3] (in MATalpha), and regulated by either the natural *PEX35* promoter (yMS2585/6) or the strong *TEF* promoter (yMS2589/90), were mated with the complementary DHFR libraries in 1536 colony array agar plates. The resulting diploids were subsequently selected for growth in the presence of methotrexate for positive DHFR PCA reconstitution for 5 days at 30°C. The colony array plates were scanned in two repeats and colony sizes were measured using the freely available Balony software (Young and Loewen, 2013), with each colony size normalized by row and column means (Table S4).

Supplementary Material

Refer to Web version on PubMed Central for supplementary material.

Acknowledgements

We thank Lihi Gal and Corinna Dickel for technical assistance, Monika Schneider and Ralph Krätzner for help with the amino acid analysis, Ariane Wolf and Anne Clancy for yeast library handling, and Hans Kristian Hannibal-Bach for assistance on lipidomics analysis. We would like to thank Ariane Wagner and Günther Daum for advice on organelle purification and for anti-Por1 antibodies, Peter Walter for anti-Kar2 antibodies and Chris Fromme for antibodies, useful discussions and ideas. We thank Nitai Steinberg for help with graphical design of figures and Jutta Gärtner for support.

Funding

This work was supported by the State of Lower-Saxony, Hannover, Germany [ZN2921 to M.S. and S.T.], and by the European Research Council [CoG 646604 to M.S.]. Maya Schuldiner is an incumbent of the Dr Gilbert Omenn and Martha Darling Professorial Chair in Molecular Genetics.

Europe PMC Funders Author Manuscripts

References

Anthonio EA, Brees C, Baumgart-Vogt E, Hongu T, Huybrechts SJ, Van Dijck P, Mannaerts GP, Kanaho Y, Van Veldhoven PP, Fransen M. Small G proteins in peroxisome biogenesis: the potential involvement of ADP-ribosylation factor 6. BMC Cell Biol. 2009; 10:58. [PubMed: 19686593]

Beach A, Burstein MT, Richard VR, Leonov A, Levy S, Titorenko VI. Integration of peroxisomes into an endomembrane system that governs cellular aging. Front Physiol. 2012; 3:283. [PubMed: 22936916]

Bernsel A, Viklund H, Falk J, Lindahl E, von Heijne G, Elofsson A. Prediction of membrane-protein topology from first principles. Proc Natl Acad Sci USA. 2008; 105:7177–7181. [PubMed: 18477697]

Brachmann CB, Davies A, Cost GJ, Caputo E, Li J, Hieter P, Boeke JD. Designer deletion strains derived from Saccharomyces cerevisiae S288C: a useful set of strains and plasmids for PCR-mediated gene disruption and other applications. Yeast. 1998; 14:115–132. [PubMed: 9483801]

Braverman NE, D'Agostino MD, MacLean GE. Peroxisome biogenesis disorders: biological, clinical and pathophysiological perspectives. Dev Disabil Res Rev. 2013; 17:187–196. [PubMed: 23798008]

Breker M, Gymrek M, Schuldiner M. A novel single-cell screening platform reveals proteome plasticity during yeast stress responses. J Cell Biol. 2013; 200:839–850. [PubMed: 23509072]

Breslow DK, Cameron DM, Collins SR, Schuldiner M, Stewart-Ornstein J, Newman HW, Braun S, Madhani HD, Krogan NJ, Weissman JS. A comprehensive strategy enabling high-resolution functional analysis of the yeast genome. Nat Methods. 2008; 5:711–718. [PubMed: 18622397]

Chelstowska A, Butow RA. RTG genes in yeast that function in communication between mitochondria and the nucleus are also required for expression of genes encoding peroxisomal proteins. J Biol Chem. 1995; 270:18141–18146. [PubMed: 7629125]

Cohen Y, Schuldiner M. Advanced methods for high-throughput microscopy screening of genetically modified yeast libraries. Methods Mol Biol. 2011; 781:127–159. [PubMed: 21877281]

Cohen Y, Klug YA, Dimitrov L, Erez Z, Chuartzman SG, Elinger D, Yofe I, Soliman K, Gärtner J, Thoms S, et al. Peroxisomes are juxtaposed to strategic sites on mitochondria. Mol Biosyst. 2014; 10:1742–1748. [PubMed: 24722918]

Colasante C, Chen J, Ahlemeyer B, Baumgart-Vogt E. Peroxisomes in cardiomyocytes and the peroxisome / peroxisome proliferator-activated receptor-loop. Thromb Haemost. 2015; 113:452–463. [PubMed: 25608554]

Copic A, Dorrington M, Pagant S, Barry J, Lee MCS, Singh I, Hartman JL, Miller EA. Genomewide analysis reveals novel pathways affecting endoplasmic reticulum homeostasis, protein modification and quality control. Genetics. 2009; 182:757–769. [PubMed: 19433630]

David C, Koch J, Oeljeklaus S, Laernsack A, Melchior S, Wiese S, Schummer A, Erdmann R, Warscheid B, Brocard C. A combined approach of quantitative interaction proteomics and live-cell imaging reveals a regulatory role for endoplasmic reticulum (ER) reticulon homology proteins in peroxisome biogenesis. Mol Cell Proteomics. 2013; 12:2408–2425. [PubMed: 23689284]

Dimitrov L, Lam SK, Schekman R. The role of the endoplasmic reticulum in peroxisome biogenesis. Cold Spring Harb Perspect Biol. 2013; 5 a013243-a013243 [PubMed: 23637287]

Dixit E, Boulant S, Zhang Y, Lee ASY, Odendall C, Shum B, Hacohen N, Chen ZJ, Whelan SP, Fransen M, et al. Peroxisomes are signaling platforms for antiviral innate immunity. Cell. 2010; 141:668–681. [PubMed: 20451243]

Donaldson JG, Jackson CL. ARF family G proteins and their regulators: roles in membrane transport, development and disease. Nat Rev Mol Cell Biol. 2011; 12:362–375. [PubMed: 21587297]

Eden E, Navon R, Steinfeld I, Lipson D, Yakhini Z. GOrilla: a tool for discovery and visualization of enriched GO terms in ranked gene lists. BMC Bioinformatics. 2009; 10:48. [PubMed: 19192299]

Effelsberg D, Cruz-Zaragoza LD, Schliebs W, Erdmann R. Pex9p is a novel yeast peroxisomal import receptor for PTS1-proteins. J Cell Sci. 2016; 129:4057–4066. [PubMed: 27678487]

Eisenberg-Bord M, Schuldiner M. Ground control to major TOM: mitochondria-nucleus communication. FEBS J. 2016; doi: 10.1111/febs13778

Ejsing CS, Sampaio JL, Surendranath V, Duchoslav E, Ekroos K, Klemm RW, Simons K, Shevchenko A. Global analysis of the yeast lipidome by quantitative shotgun mass spectrometry. Proc Natl Acad Sci USA. 2009; 106:2136–2141. [PubMed: 19174513]

Elbaz-Alon Y, Morgan B, Clancy A, Amoako TNE, Zalckvar E, Dick TP, Schwappach B, Schuldiner M. The yeast oligopeptide transporter Opt2 is localized to peroxisomes and affects glutathione redox homeostasis. FEMS Yeast Res. 2014; 14:1055–1067. [PubMed: 25130273]

Emanuelsson O, Brunak S, von Heijne G, Nielsen H. Locating proteins in the cell using TargetP, SignalP and related tools. Nat Protoc. 2007; 2:953–971. [PubMed: 17446895]

Eubel H, Meyer EH, Taylor NL, Bussell JD, O'Toole N, Heazlewood JL, Castleden I, Small ID, Smith SM, Millar AH. Novel proteins, putative membrane transporters, and an integrated metabolic network are revealed by quantitative proteomic analysis of Arabidopsis cell culture peroxisomes. Plant Physiol. 2008; 148:1809–1829. [PubMed: 18931141]

Flis VV, Fankl A, Ramprecht C, Zellnig G, Leitner E, Hermetter A, Daum G. Phosphatidylcholine Supply to Peroxisomes of the Yeast Saccharomyces cerevisiae. PLoS One. 2015; 10 e0135084 [PubMed: 26241051]

Fransen M, Nordgren M, Wang B, Apanasets O, Van Veldhoven PP. Aging, age-related diseases and peroxisomes. Subcell Biochem. 2013; 69:45–65. [PubMed: 23821142]

Fukao Y, Hayashi M, Nishimura M. Proteomic analysis of leaf peroxisomal proteins in greening cotyledons of Arabidopsis thaliana. Plant Cell Physiol. 2002; 43:689–696. [PubMed: 12154131]

Giaever G, Chu AM, Ni L, Connelly C, Riles L, Véronneau S, Dow S, Lucau-Danila A, Anderson K, André B, et al. Functional profiling of the Saccharomyces cerevisiae genome. Nature. 2002; 418:387–391. [PubMed: 12140549]

Gietz RD, Woods RA. Yeast transformation by the LiAc/SS Carrier DNA/PEG method. Methods Mol Biol. 2006; 313:107–120. [PubMed: 16118429]

Göttfert F, Wurm CA, Mueller V, Berning S, Cordes VC, Honigmann A, Hell SW. Coaligned dual-channel STED nanoscopy and molecular diffusion analysis at20 nm resolution. Biophys J. 2013; 105:L01–L03. [PubMed: 23823248]

Gronemeyer T, Wiese S, Ofman R, Bunse C, Pawlas M, Hayen H, Eisenacher M, Stephan C, Meyer HE, Waterham HR, et al. The proteome of human liver peroxisomes: identification of five new peroxisomal constituents by a label-free quantitative proteomics survey. PLoS ONE. 2013; 8 e57395 [PubMed: 23460848]

Huh W-K, Falvo JV, Gerke LC, Carroll AS, Howson RW, Weissman JS, O'Shea EK. Global analysis of protein localization in budding yeast. Nature. 2003; 425:686–691. [PubMed: 14562095]

Huhse B, Rehling P, Albertini M, Blank L, Meller K, Kunau W-H. Pex17p of Saccharomyces cerevisiae is a novel peroxin and component of the peroxisomal protein translocation machinery. J Cell Biol. 1998; 140:49–60. [PubMed: 9425153]

Islinger M, Lüers GH, Li KW, Loos M, Völkl A. Rat liver peroxisomes after fibrate treatment A survey using quantitative mass spectrometry. J Biol Chem. 2007; 282:23055–23069. [PubMed: 17522052]

Islinger M, Li KW, Loos M, Liebler S, AngerMüller S, Eckerskorn C, Weber G, Abdolzade A, Völkl A. Peroxisomes from the heavy mitochondrial fraction: isolation byzonal free flow electrophoresis and quantitative mass spectrometrical characterization. J Proteome Res. 2010; 9:113–124. [PubMed: 19739631]

Islinger M, Grille S, Fahimi HD, Schrader M. The peroxisome: an update on mysteries. Histochem Cell Biol. 2012; 137:547–574. [PubMed: 22415027]

Jackson CL, Bouvet S. Arfs at a glance. J Cell Sci. 2014; 127:4103–4109. [PubMed: 25146395]

Janke C, Magiera MM, Rathfelder N, Taxis C, Reber S, Maekawa H, Moreno-Borchart A, Doenges G, Schwob E, Schiebel E, et al. A versatile tool box for PCR-based tagging of yeast genes: new fluorescent proteins, more markers and promoter substitution cassettes. Yeast. 2004; 21:947–962. [PubMed: 15334558]

Jian X, Cavenagh M, Gruschus JM, Randazzo PA, Kahn RA. Modifications to the C-terminus of Arf1 alter cell functions and protein interactions. Traffic. 2010; 11:732–742. [PubMed: 20214751]

Just, W, Kunau, W-H. History and discovery of peroxinsMolecular Machines Involved in Peroxisome Biogenesis and Maintenance. Brocard, C, Hartig, A, editors. Springer; Vienna: 2014. 3–15.

Kaplan C, Ewers H. Optimized sample preparation for single-molecule localization-based super resolution microscopy in yeast. Nat Protoc. 2015; 10:1007–1021. [PubMed: 26068895]

Kettelhut, T, Thoms, S. Expanding the clinical phenotypes of peroxisome biogenesis disorders: PEX11 function in health and diseaseMolecular Machines Involved in Peroxisome Biogenesis and Maintenance. Springer; 2014. 111–123.

Kikuchi M, Hatano N, Yokota S, Shimozawa N, Imanaka T, Taniguchi H. Proteomic analysis of rat liver peroxisome: presence of peroxisome-specific isozyme of Lon protease. J Biol Chem. 2004; 279:421–428. [PubMed: 14561759]

Krogh A, Larsson B, von Heijne G, Sonnhammer ELL. Predicting transmembrane protein topology with a hidden Markov model: application to complete genomes. J Mol Biol. 2001; 305:567–580. [PubMed: 11152613]

Lay D, Grosshans BL, Heid H, Gorgas K, Just WW. Binding and functions of ADP-ribosylation factor on mammalian and yeast peroxisomes. J Biol Chem. 2005; 280:34489–34499. [PubMed: 16100119]

Lay D, Gorgas K, Just WW. Peroxisome biogenesis: where Arf and coatomer might be involved. Biochim Biophys Acta. 2006; 1763:1678–1687. [PubMed: 17023067]

Lockshon D, Surface LE, Kerr EO, Kaeberlein M, Kennedy BK. The sensitivity of yeast mutants to oleic acid implicates the peroxisome and other processes in membrane function. Genetics. 2007; 175:77–91. [PubMed: 17151231]

Longtine MS, McKenzie A III, Demarini DJ, Shah NG, Wach A, Brachat A, Philippsen P, Pringle JR. Additional modules for versatile and economical PCR-based gene deletion and modification in Saccharomyces cerevisiae. Yeast. 1998; 14:953–961. [PubMed: 9717241]

Mãgalhaes AC, Ferreira AR, Gomes S, Vieira M, Gouveia A, Valenca I, Islinger M, Nascimento R, Schrader M, Kagan JC, et al. Peroxisomes are platforms for cytomegalovirus' evasion from the cellular immune response. Sci Rep. 2016; 6 26028 [PubMed: 27181750]

Maier AG, Schulreich S, Bremser M, Clayton C. Binding of coatomer by the PEX11 C-terminus is not required for function. FEBS Lett. 2000; 484:82–86. [PubMed: 11068037]

Marelli M, Smith JJ, Jung S, Yi E, Nesvizhskii AI, Christmas RH, Saleem RA, Tam YYC, Fagarasanu A, Goodlett DR, et al. Quantitative mass spectrometry reveals a role for the GTPase Rho1p in actin organization on the peroxisome membrane. J Cell Biol. 2004; 167:1099–1112. [PubMed: 15596542]

McCartney AW, Greenwood JS, Fabian MR, White KA, Mullen RT. Localization of the tomato bushystuntvirus replication protein p33 reveals a peroxisome-to-endoplasmic reticulum sorting pathway. Plant Cell. 2005; 17:3513–3531. [PubMed: 16284309]

Mi J, Kirchner E, Cristobal S. Quantitative proteomic comparison of mouse peroxisomes from liver and kidney. Proteomics. 2007; 7:1916–1928. [PubMed: 17474143]

Mohanty A, McBride HM. Emerging roles of mitochondria in the evolution, biogenesis, and function of peroxisomes. Front Physiol. 2013; 4:268. [PubMed: 24133452]

Morgan B, Sobotta MC, Dick TP. Measuring E(GSH) and H2O2 with roGFP2-based redox probes. Free Radic Biol Med. 2011; 51:1943–1951. [PubMed: 21964034]

Natarajan K, Meyer MR, Jackson BM, Slade D, Roberts C, Hinnebusch AG, Marton MJ. Transcriptional profiling shows that Gcn4p is a master regulator of gene expression during amino acid starvation in yeast. Mol Cell Biol. 2001; 21:4347–4368. [PubMed: 11390663]

Nötzel C, Lingner T, Klingenberg H, Thoms S. Identification of new fungal peroxisomal matrix proteins and revision of the PTS1 consensus. Traffic. 2016; 17:1110–1124. [PubMed: 27392156]

Odendall C, Dixit E, Stavru F, Bierne H, Franz KM, Durbin AF, Boulant S, Gehrke L, Cossart P, Kagan JC. Diverse intracellular pathogens activate type III interferon expression from peroxisomes. Nat Immunol. 2014; 15:717–726. [PubMed: 24952503]

Ofman R, Speijer D, Leen R, Wanders RJA. Proteomic analysis of mouse kidney peroxisomes: identification of RP2p as a peroxisomal nudix hydrolase with acyl-CoA diphosphatase activity. Biochem J. 2006; 393:537–543. [PubMed: 16185196]

Passreiter M, Anton M, Lay D, Frank R, Harter C, Wieland FT, Gorgas K, Just WW. Peroxisome biogenesis: involvement of ARF and coatomer. J Cell Biol. 1998; 141:373–383. [PubMed: 9548716]

Reumann S, Babujee L, Ma C, Wienkoop S, Siemsen T, Antonicelli GE, Rasche N, Lüder F, Weckwerth W, Jahn O. Proteome analysis of Arabidopsis leaf peroxisomes reveals novel targeting peptides, metabolic pathways, and defense mechanisms. Plant Cell. 2007; 19:3170–3193. [PubMed: 17951448]

Reumann S, Quan S, Aung K, Yang P, Manandhar-Shrestha K, Holbrook D, Linka N, Switzenberg R, Wilkerson CG, Weber APM, et al. In-depth proteomeanalysis of Arabidopsis leaf peroxisomes combined with in vivo subcellular targeting verification indicates novel metabolic and regulatory functions of peroxisomes. Plant Physiol. 2009; 150:125–143. [PubMed: 19329564]

Rucktaschel R, Thoms S, Sidorovitch V, Halbach A, Pechlivanis M, Volkmer R, Alexandrov K, Kuhlmann J, Rottensteiner H, Erdmann R. Farnesylation of pex19p is required for its structural integrity and function in peroxisome biogenesis. J Biol Chem. 2009; 284:20885–20896. [PubMed: 19451657]

Saleem RA, Knoblach B, Mast FD, Smith JJ, Boyle J, Dobson CM, Long-O'Donnell R, Rachubinski RA, Aitchison JD. Genome-wide analysis of signaling networks regulating fatty acid-induced gene expression and organelle biogenesis. J Cell Biol. 2008; 181:281–292. [PubMed: 18426976]

Saleem RA, Long-O'Donnell R, Dilworth DJ, Armstrong AM, Jamakhandi AP, Wan Y, Knijnenburg TA, Niemistö A, Boyle J, Rachubinski RA, et al. Genome-wide analysis of effectors of peroxisome biogenesis. PLoS ONE. 2010; 5 e11953 [PubMed: 20694151]

Schäfer H, Nau K, Sickmann A, Erdmann R, Meyer HE. Identification of peroxisomal membrane proteins of Saccharomyces cerevisiae by mass spectrometry. Electrophoresis. 2001; 22:2955–2968. [PubMed: 11565790]

Schrader M, Grille S, Fahimi HD, Islinger M. Peroxisome interactions and cross-talk with other subcellular compartments in animal cells. Subcell Biochem. 2013; 69:1–22. [PubMed: 23821140]

Smith JJ, Aitchison JD. Peroxisomes take shape. Nat Rev Mol Cell Biol. 2013; 14:803–817. [PubMed: 24263361]

Smith JJ, Marelli M, Christmas RH, Vizeacoumar FJ, Dilworth DJ, Ideker T, Galitski T, Dimitrov K, Rachubinski RA, Aitchison JD. Transcriptome profiling to identify genes involved in peroxisome assembly and function. J Cell Biol. 2002; 158:259–271. [PubMed: 12135984]

Smith JJ, Sydorskyy Y, Marelli M, Hwang D, Bolouri H, Rachubinski RA, Aitchison JD. Expression and functional profiling reveal distinct gene classes involved in fatty acid metabolism. Mol Syst Biol. 2006; 2 2006.0009

South ST, Sacksteder KA, Li X, Liu Y, Gould SJ. Inhibitors of COPI and COPII do not block PEX3-mediated peroxisome synthesis. J Cell Biol. 2000; 149:1345–1360. [PubMed: 10871277]

Stearns T, Willingham MC, Botstein D, Kahn RA. ADP-ribosylation factor is functionally and physically associated with the Golgi complex. Proc Natl Acad Sci USA. 1990; 87:1238–1242. [PubMed: 2105501]

Tarassov K, Messier V, Landry CR, Radinovic S, Serna Molina MM, Shames I, Malitskaya Y, Vogel J, Bussey H, Michnick SW. An in vivo map of the yeast protein interactome. Science. 2008; 320:1465–1470. [PubMed: 18467557]

Thoms S, Erdmann R. Dynamin-related proteins and Pex11 proteins in peroxisome division and proliferation. FEBS J. 2005; 272:5169–5181. [PubMed: 16218949]

Thoms S, Gärtner J. First PEX11β patient extends spectrum of peroxisomal biogenesis disorder phenotypes. J Med Genet. 2012; 49:314–316. [PubMed: 22581969]

Thoms S, Debelyy MO, Nau K, Meyer HE, Erdmann R. Lpx1p is a peroxisomal lipase required fornormal peroxisome morphology. FEBS J. 2008; 275:504–514. [PubMed: 18199283]

Thoms S, Gønborg S, Gärtner J. Organelle interplay in peroxisomal disorders. Trends Mol Med. 2009; 15:293–302. [PubMed: 19560974]

Thoms S, Harms I, Kalies K-U, Gärtner J. Peroxisome formation requires the endoplasmic reticulum channel protein Sec61. Traffic. 2011a; 13:599–609.

Thoms S, Debelyy M, Connerth M, Daum G, Erdmann R. The putative Saccharomyces cerevisiae hydrolase Ldh1p is localized to lipid droplets. Eukaryot Cell. 2011b; 10:770–775. [PubMed: 21478430]

Tong AHY, Boone C. Synthetic genetic array analysis in Saccharomyces cerevisiae. Methods Mol Biol. 2006; 313:171–192. [PubMed: 16118434]

Tower RJ, Fagarasanu A, Aitchison JD, Rachubinski RA. The peroxin Pex34p functions with the Pex11 family of peroxisomal divisional proteins to regulate the peroxisome population in yeast. Mol Biol Cell. 2011; 22:1727–1738. [PubMed: 21441307]

Trompier D, Vejux A, Zarrouk A, Gondcaille C, Geillon F, Nury T, Savary S, Lizard G. Brain peroxisomes. Biochimie. 2014; 98:102–110. [PubMed: 24060512]

van der Zand A, Braakman I, Tabak HF. Peroxisomal membrane proteins insert into the endoplasmic reticulum. Mol Biol Cell. 2010; 21:2057–2065. [PubMed: 20427571]

Voorn-Brouwer T, Kragt A, Tabak HF, Distel B. Peroxisomal membrane proteins are properly targeted to peroxisomes in the absence of COPI-and COPII-mediated vesicular transport. J Cell Sci. 2001; 114:2199–2204. [PubMed: 11493655]

Wanders RJA, Waterham HR. Biochemistry of mammalian peroxisomes revisited. Annu Rev Biochem. 2006; 75:295–332. [PubMed: 16756494]

Weller S, Gould SJ, Valle D. Peroxisome biogenesis disorders. Annu Rev Genomics Hum Genet. 2003; 4:165–211. [PubMed: 14527301]

Wiese S, Gronemeyer T, Ofman R, Kunze M, Grou CP, Almeida JA, Eisenacher M, Stephan C, Hayen H, Schollenberger L, et al. Proteomics characterization of mouse kidney peroxisomes by tandem mass spectrometryand protein correlation profiling. Mol Cell Proteomics. 2007; 6:2045–2057. [PubMed: 17768142]

Wolinski H, Petrovič U, Mattiazzi M, Petschnigg J, Heise B, Natter K, Kohlwein SD. Imaging-based live cell yeast screen identifies novel factors involved in peroxisome assembly. J Proteome Res. 2009; 8:20–27. [PubMed: 19118449]

Yi EC, Marelli M, Lee H, Purvine SO, Aebersold R, Aitchison JD, Goodlett DR. Approaching complete peroxisome characterization by gas-phase fractionation. Electrophoresis. 2002; 23:3205–3216. [PubMed: 12298092]

Yifrach E, Chuartzman SG, Dahan N, Maskit S, Zada L, Weill U, Yofe I, Olender T, Schuldiner M, Zalckvar E. Characterization of proteome dynamics in oleate reveals a novel peroxisome targeting receptor. J Cell Sci. 2016; 129:4067–4075. [PubMed: 27663510]

Yofe I, Schüldiner M. Primers-4-Yeast: a comprehensive web tool for planning primers for Saccharomyces cerevisiae. Yeast. 2014; 31:77–80. [PubMed: 24408512]

Yofe I, Weill U, Meurer M, Chuartzman S, Zalckvar E, Goldman O, Ben-Dor S, Schu tze C, Wiedemann N, Knop M, et al. One library to make them all:streamlining the creation of yeast libraries via a SWAp-Tag strategy. Nat Methods. 2016; 13:371–378. [PubMed: 26928762]

Young BP, Loewen CJR. Balony: a software package for analysis of data generated by synthetic genetic array experiments. BMC Bioinformatics. 2013; 14:354. [PubMed: 24305553]

Europe PMC Funders Author Manuscripts

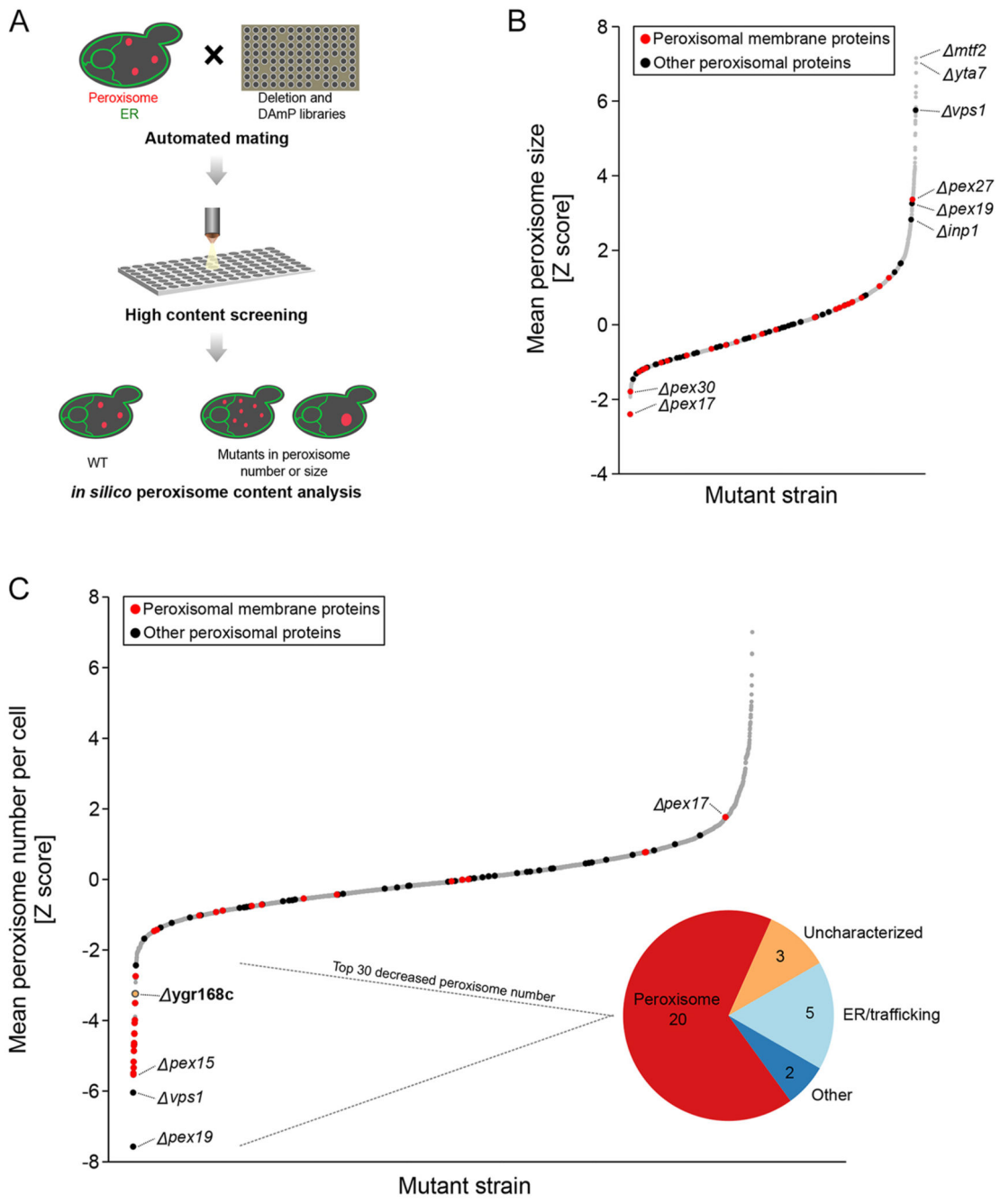

Fig. 1. A high-content screen uncovers regulators of peroxisome size and number.

(A) Schematic representation of the high-content screen workflow. A query strain containing the peroxisomal marker Pex3-mCherry and the ER marker Spf1-GFP was crossed with strain collections of gene deletions and hypomorphic alleles. Following selection, the resulting haploid yeast each contained both a single mutation and the markers. The libraries were imaged using a high-throughput automated microscope. Images were analyzed by software-assisted single-cell and object (peroxisome) recognition, allowing the identification of mutants that show aberrant peroxisome size or number. (B) Distribution of the Z score of

the mean peroxisome size for successfully analyzed mutant strains. Mutants of peroxisomal membrane proteins are marked in red, and other peroxisomal proteins marked in black. (C) Distribution of the Z score of the mean peroxisome number per cell for successfully analyzed mutant strains. A high enrichment of peroxisomal membrane protein mutants and *Δpex* mutants is found in the group of decreased peroxisome number, as illustrated by the inset pie chart, presenting functional classes of the 30 mutants in this group. *YGR168C* is a previously uncharacterized gene found within this group. Mutants of peroxisomal membrane proteins are marked in red, and other peroxisomal proteins are marked in black.

Europe PMC Funders Author Manuscripts

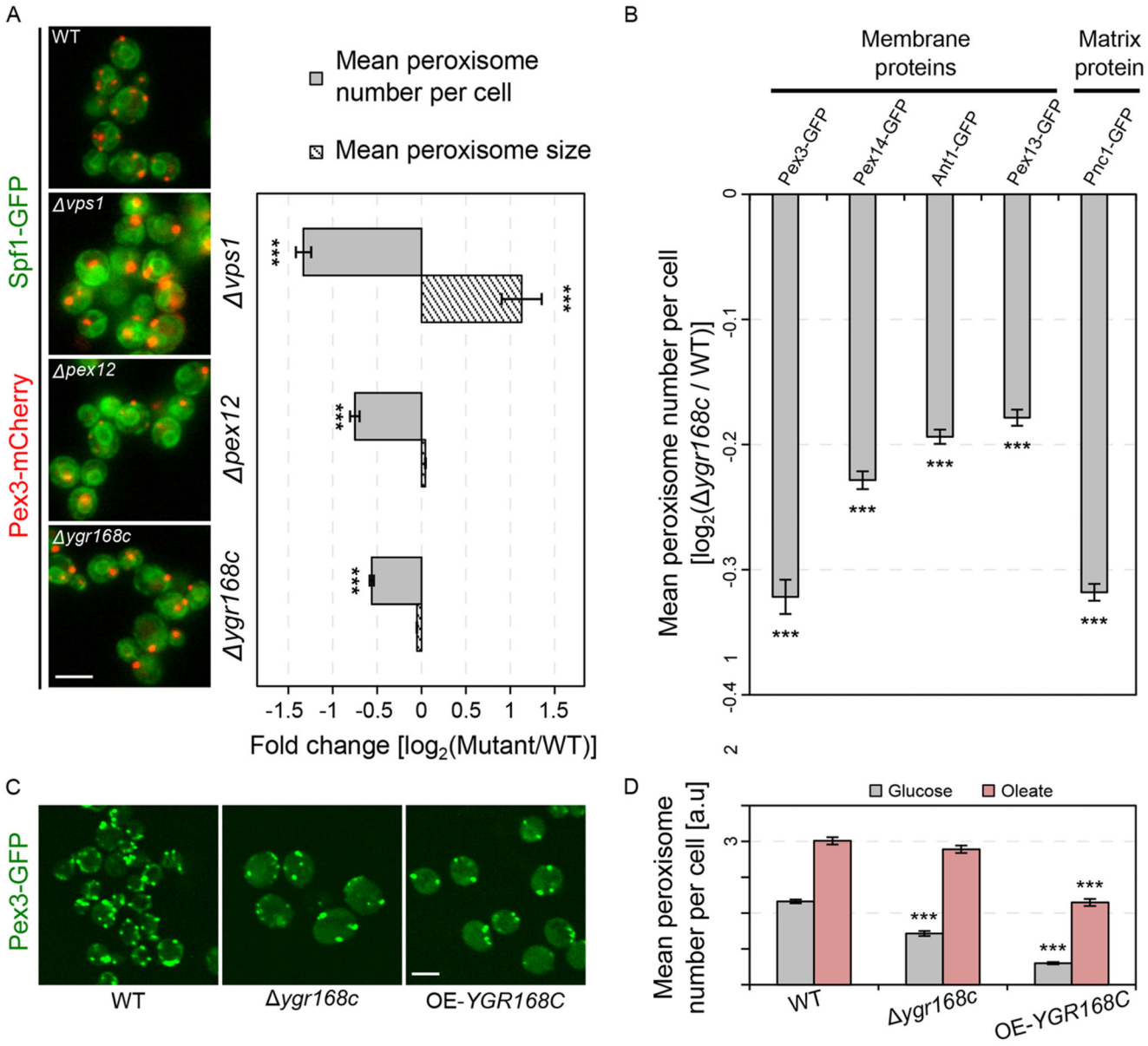

Fig. 2. Deletion or overexpression of *YGR168C* affects peroxisome number and function.

(A) Examples of mutants from the high-content screen showing aberrant peroxisome content. Images of strains from the high-content screen containing Pex3-RFP and Spf1-GFP. Peroxisome size is increased in *Δvps1*, and peroxisome number is decreased in *Δvps1, Δpex12* and *Δygr168c*, compared to a wild-type (WT) strain. Scale bar: 5 μm. Graph shows quantification of these parameters (see also Fig. S1). n>72, ***P<0.01 compared with WT (t-test). (B) Reduction in peroxisome number in *Δygr168c* is independent of the peroxisomal marker used. The number of peroxisomes per cell was analyzed by using several peroxisomal membrane or matrix proteins tagged with GFP, either in a WT or*Δygr168c* background. The decrease in peroxisome number in *Δygr168c* is seen with all peroxisome markers used, n=6. ***P<0.01 *(Δygr168c* versus WT; t-testforeach marker). (C)

Overexpression of *YGR168C* reduces thenumberofperoxisome puncta. Images of strains with Pex3-GFP and that are WT, *Δygr168c* or overexpress *YGR168C (OE-YGR168C)*. Scale bar: 5 μm. (D) Peroxisome number is affected in *ygr168c* mutants grown in glucose and oleate. Quantification of mean cell peroxisome number per cell in WT, *Δygr168c, or OE-YGR168C* cells, visualized aftergrowth in either glucose (gray) or oleate (red) medium. While an increase in peroxisome number is observed in oleate compared to glucose foreach strain, peroxisome number is decreased in the mutants compared to WT in glucose medium, and in OE-YGR168C in oleate. n>73l. ***P<0.01 compared with the same medium for WT (t-test). All quantitative data are mean±s.e.m.

Europe PMC Funders Author Manuscripts

Europe PMC Funders Author Manuscripts

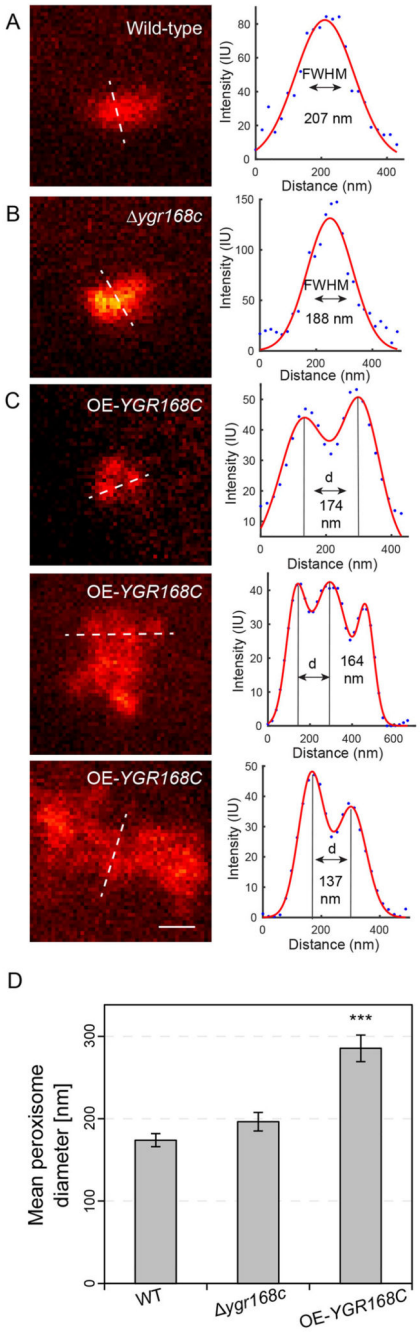

Fig. 3. STED microscopy reveals characteristics of wild-type and *ygr168c* peroxisomes.

(A-C) Examples of STED super-resolution microscopy of wildtype (WT; A), *Δygr168c* (B) and strains overexpressing *YGR168C* (OE-*YGR168C;* C) expressing EYFP-SKL as a peroxisomal marker and labeled with anti-GFP nanobodies. Scale bar: 200 nm. The size of peroxisomes was determined as the FWHM of a Gaussian fit. Dashed lines, positions of size and cluster measurements. Peroxisome diameter in *Δygr168c* is not altered. Overexpression of *YGR168C* causes an increase in the apparent size of peroxisomes. In conventional light microscopy, these aggregates appear as enlarged single peroxisomes. Sub-diffraction

imaging reveals that enlarged peroxisomes consist of multi-lobular structures, whereby the individual substructures appear as peroxisomes of wild-type-like morphology. The distances between the maxima varies between 137 and 174 nm. (D) The mean diameter of WT peroxisomes is 174±8 nm (s.e.m.). The size difference between wild-type and knockout peroxisomes 96±7 nm (s.e.m.) was not significant (P=0.1). The mean diameter of OE-YGR168C peroxisome clusters is 285 nm (±16 nm s.e.m.) (***$P=6\times10^{-8}$ compared with WT). n>50 in all cases.

Europe PMC Funders Author Manuscripts

Europe PMC Funders Author Manuscripts

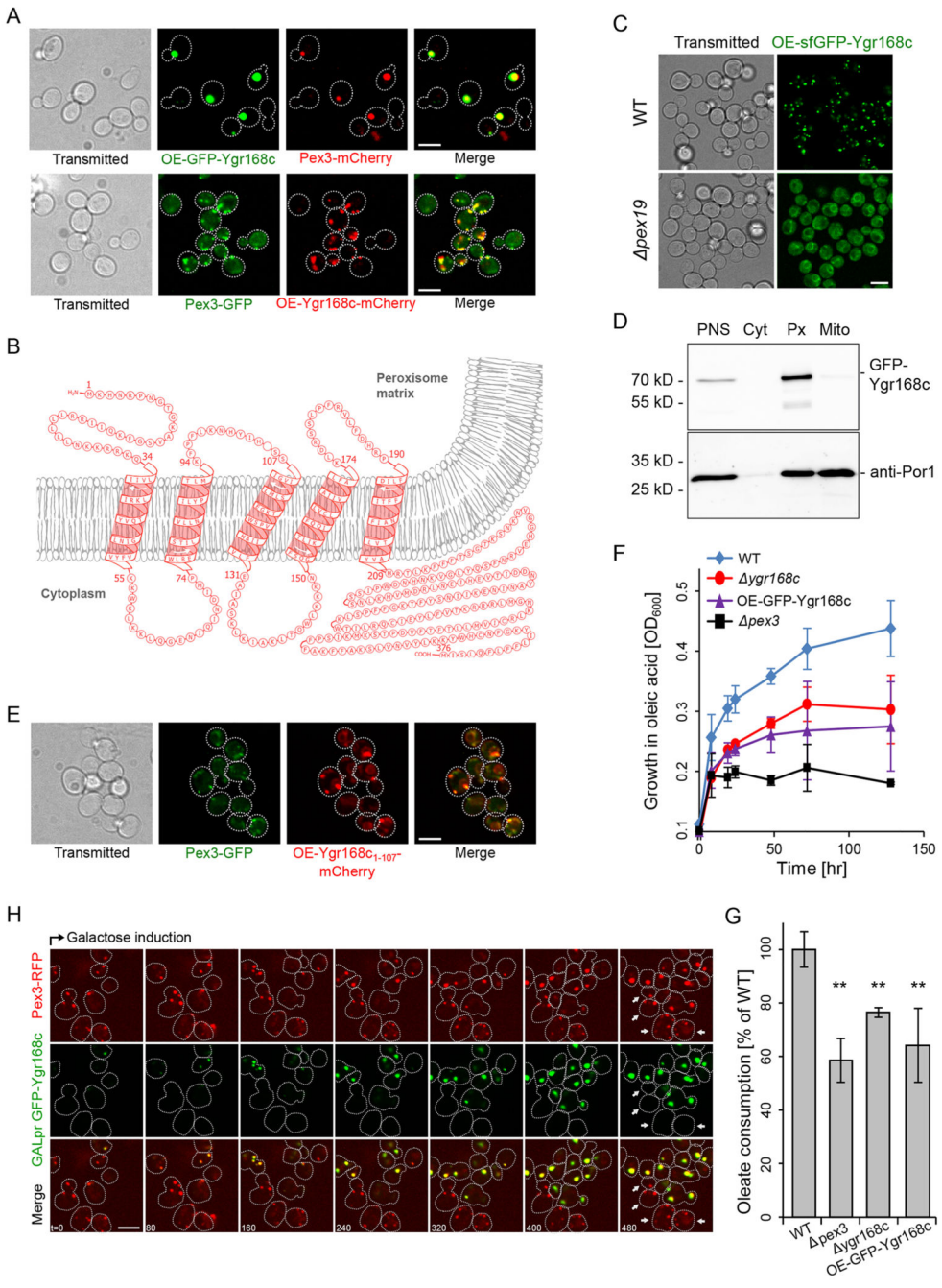

Fig. 4. *YGR168C (PEX35)* is a new *PEX* gene.

(A) Ygr168c colocalizes with a peroxisomal marker. Overexpressed (OE) N-terminally GFP-tagged Ygr168c colocalizes with Pex3-mCherry, with a notable phenotype of about one large peroxisome per cell (top). Overexpression of Ygr168c with a C-terminal mCherry tag displays colocalization with Pex3-GFP (bottom) with wild-type (WT) peroxisome abundance. Scale bars: 5 μm. (B) Predicted transmembrane topology of Ygr168c (Pex35). Transmembrane helices were predicted by the TMHMM algorithm (v2.0). The schematic representation demonstrates the five transmembrane domains, as well as a long cytoplasmic

C-terminus for the protein. (C) Deletion of *PEX19* leads to the cytosolic localization and ER accumulation of Ygr168c. sfGFP, superfolder GFP. Scale bar: 5 μm. (D) Identification of GFP-Ygr168c on purified wild-type peroxisomes isolated from oleate-induced cells. Western blot analysis of the post-nuclear supernatant (PNS), and cytosol (Cyt), peroxisomal (Px) and mitochondrial (Mito) fractions from the Nycodenz step gradient. Anti-Por1 antibody is used as a mitochondrial marker. (E) Overexpression of amino acids 1-107 of Ygr168c ($Ygr168c_{1-107}$; including the N-terminal region and the first two predicted transmembrane domains) tagged with mCherry displays colocalization with Pex3-GFP, and also shows localization to the ER. Scale bar: 5 μm. (F) *YGR168C* mutants grow more slowly in medium containing oleic acid as the sole carbon source. WT, *Δygr168c, OE-YGR168C* and *Δpex3* strains were grown in oleic acid for 128 h, and the OD_{600} was measured to assess growth. *YGR168C* mutants display a significant growth defect, at an intermediate level between WT and the *Δpex3*. Error bars indicate s.d., n=4. (G) *YGR168C* mutants consume less oleic acid. Media from the end-point of the experiment described in D (128 h) were used to assess the relative oleic acid consumption of each strain. Error bars indicate s.d., n=4. ** $P<0.05$ (*t*-test). (H) Induction of GFP-Ygr168c leads to accumulation of the protein in peroxisomes, and to aberrant peroxisome content. A strain expressing both Pex3-RFP and GFP-Ygr168c under the control of the inducible *GAL1* promoterwas transferred from glucose to galactose medium. Time-lapse imaging was carried out starting from 90 min (*t*=0). GFP-Ygr168c becomes highly induced under these conditions and colocalizes with Pex3-RFP over time. Notably, cells in which GFP-Ygr168c is not expressed (arrows) display normal peroxisome content, while cells in which expression is induced display one large peroxisome in each cell. Scale bar: 5 μm. Dashed lines in images highlight cell outlines.

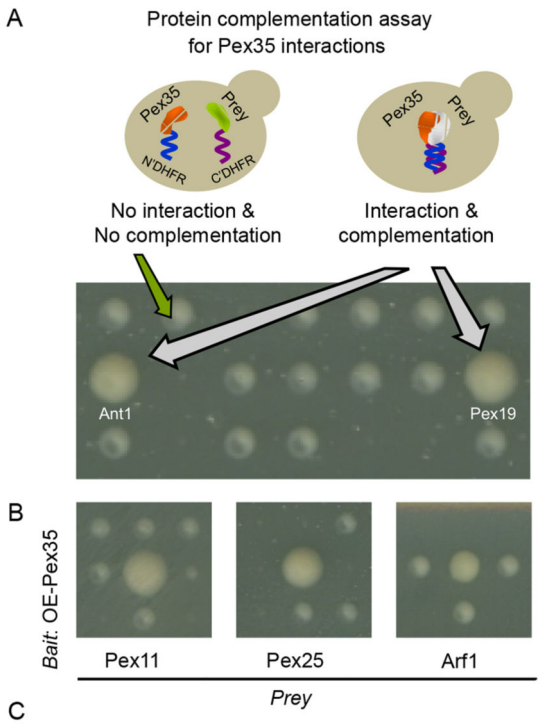

C

Ranking	Gene	Protein Name	Fold increase colony size
1	*YOL147C*	Pex11	8.0
2	*YPL112C*	Pex25	5.4
3	*YDL065C*	Pex19	3.8
5	*YDR329C*	Pex3	3.1
6	*YDL192W*	Arf1	2.7
7	*YPR128C*	Ant1	2.6
8	*YLR191W*	Pex13	2.6
9	*YPL186C*	Uip4	2.5
10	*YGR168C*	Pex35	2.4
11	*YMR026C*	Pex12	2.3
12	*YIR038C*	Gtt1	2.3
14	*YBL039W-B*		2.1
15	*YCL056C*	Pex34	2.1
16	*YDR265W*	Pex10	2.1
17	*YPR097W*		2.1

Fig. 5. Pex35 is found in proximity to peroxisomal membrane proteins as well as to Arf proteins.
(A) A protein complementation assay for Pex35 interactions reveals a physical proximity to the Pex11, Pex25 and Arf1. Query strains with Pex35 tagged with either the C- or N-terminal fragment of the DHFR enzyme were mated with collections of strains expressing the other half of DHFR in the opposing mating type. Interaction between the Pex35 (bait) and a screened protein (prey) results in complementation of the DHFR enzyme, which in turn enables growth on the methotrexate medium, as shown for Ant1 and Pex19. (B) Pex35 is in proximity to Pex11, Pex25 and Arf1. Each of the three indicated Pex35-prey

combinations, shown in the center of each image, display large colonies, in contrast to the neighboring colonies with other Pex35-prey combinations. (C) Summary of proteins in proximity to Pex35. Fold increase colony size: the maximum colony size of four combinations of the DHFR screen (overexpression or native promoter for *PEX35* bait, and two DHFR fragment collections).

Europe PMC Funders Author Manuscripts

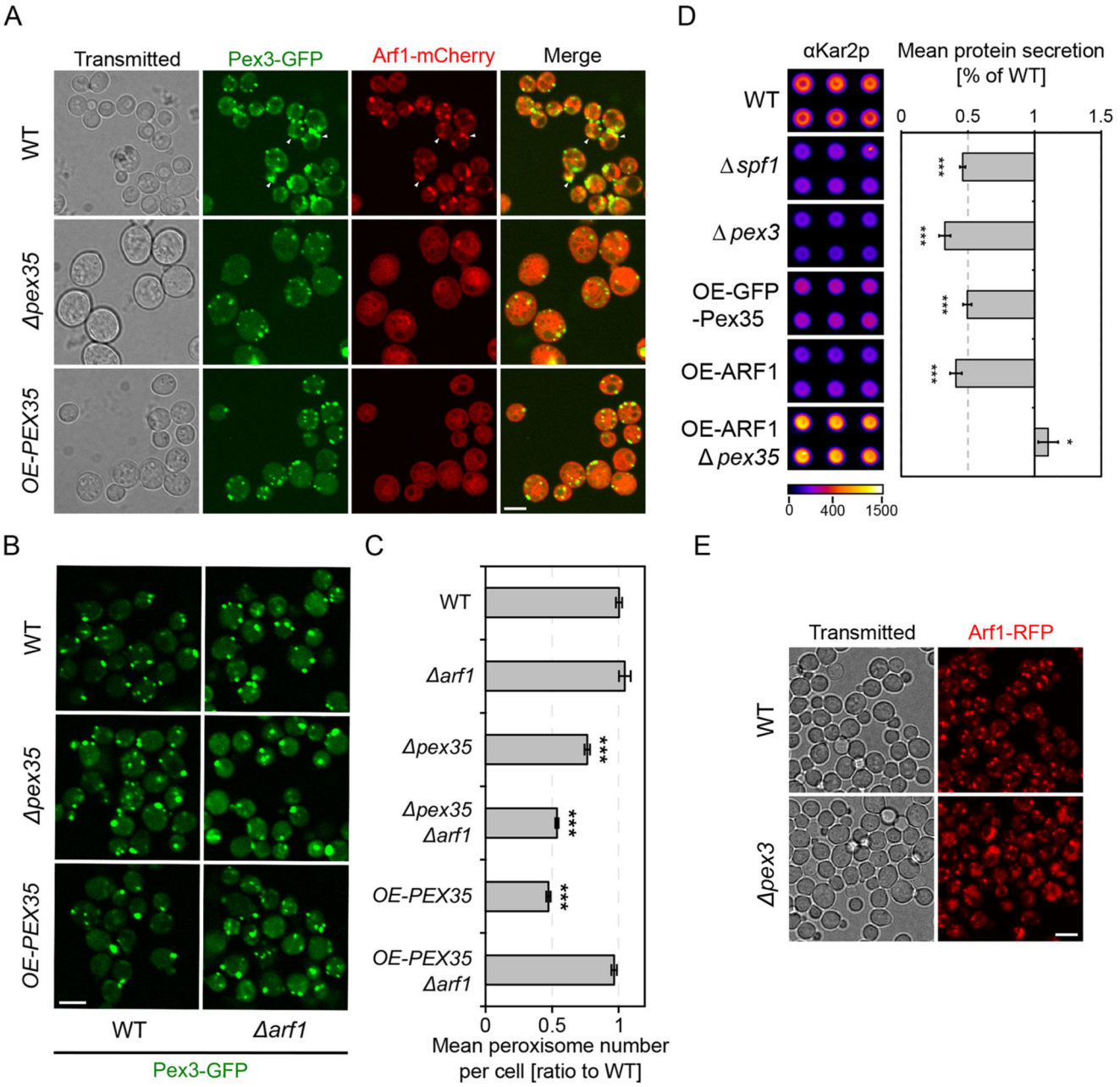

Fig. 6. Pex35 and peroxisomes control Arf1 distribution and function.

(A) Arf1 distribution is impaired in *pex35* mutants. While Arf1-RFP is localized in punctate structures (potentially including Golgi and mitochondria) and partially colocalizes to peroxisomes (white arrowheads) in wild-type (WT) strains, deletion or overexpression (OE) of PEX35 results in re-distribution to other internal membranes and loss of punctate localization. Scale bar: 5 μm. (B) Synthetic effects of *PEX35* and *ARF1* mutations. Pex3-GFP was used as a marker to quantify the peroxisome abundance in combinations of *Δarf1* and WT, *Δpex35 or OE-PEX35*. Scale bar: 5 μm. (C) Quantification of peroxisomal content reveals that deletion of *ARF1* aggravates the *Δpex35* phenotype of reduced peroxisome

number. Notably, *Δarf1* deletion compensated for the effect of *PEX35* overexpression on peroxisome abundance. Error bars indicate s.e.m., n>197. ***P<0.01 compared with WT (*t*-test). (D) Protein secretion analysis of *PEX35* and *ARF1* mutants. Images (left; the levels of secretion of Kar2 are indicated) and quantification (right) of a western blot of Kar2 secreted from six colony repeats per strain. Induction of the UPR (by deletion of *SPF1)* or loss of peroxisomes (by deletion of *PEX3)*, as well as overexpression of GFP-Pex35 or *ARF1* significantly reduced secretion levels. Deletion of *PEX35* compensated for the effect of *ARF1* overexpression. Error bars indicate s.d., n=6. *P<0.1 (not significant); ***P<0.01 (*t*-test). (E) Deletion of *PEX3* affects cellular Arf1-RFP distribution. In*Δpex3* cells, Arf1-RFP loses its localization to defined puncta. Scale bar: 5 μm.

Europe PMC Funders Author Manuscripts

Europe PMC Funders Author Manuscripts

Table 1

Top hits of the microscopic screen for proteins involved in peroxisome formation

Rank	Gene	Protein	Abundance
1	*YDL065C*	Pex19	−7.6
2	*YKR001C*	Vps1	−6.0
3	*YOL044W*	Pex15	−5.5
4	*YNL329C*	Pex6	−5.5
5	*YOR193W*	Pex27	−5.3
6	*YKL197C*	Pex1	−5.2
7	*YDR265W*	Pex10	−4.9
8	*YMR204C*	Inp1	−4.7
9	*YGR077C*	Pex8	−4.7
10	*YJL210W*	Pex2	−4.6
11	*YCL056C*	Pex34	−4.4
12	*YPL112C*	Pex25	−4.4
13	*YMR026C*	Pex12	−4.1
14	*YMR205C*	Pfk2	−4.0
15	*YMR163C*	Inp2	−4.0
16	*YLR191W*	Pex13	−3.5
17	*YGR168C*		−3.2
18	*YDR233C*	Rtn1	−2.9
19	*YLR126C*		−2.8
20	*YPR128C*	Ant1	−2.7
21	*YOR084W*	Lpx1	−2.4

Abundance: peroxisome number per cell (Z score).

Europe PMC Funders Author Manuscripts

Table 2
Top hits of the PEX35 synthetic genetic interactions screen

Rank	Gene	Protein	SM	DM	DM/SM
1	*YOR130C*	Ort1	0.86	0.24	0.27
2	*YKL184W*	Spe1	0.67	0.19	0.29
3	*YNL268W*	Lyp1	0.13	0.04	0.34
4	*YCR028C-A*	Rim1	0.12	0.05	0.39
5	*YDR234W*	Lys4	0.81	0.32	0.40
6	*YJL101C*	Gsh1	0.22	0.11	0.47
7	*YBR081C*	Spt7	0.20	0.10	0.48
8	*YJL071W*	Arg2	0.21	0.11	0.51
9	*YNL270C*	Alp1	1.30	0.69	0.53
10	*YER116C*	Slx8	0.25	0.14	0.54
11	*YGL143C*	Mrf1	0.49	0.28	0.57
12	*YBR251W*	Mrps5	0.13	0.07	0.57
13	*YNL005C*	Mrp7	0.30	0.17	0.58
14	*YHR147C*	Mrpl6	0.19	0.11	0.61
15	*YER185W*	Pug1	1.51	0.94	0.62
16	*YGL076C*	Rpl7a	0.49	0.31	0.63
17	*YMR142C*	Rpl13b	0.49	0.32	0.65
18	*YPR099C*	Ypr099c	0.30	0.20	0.66
19	*YDR028C*	Reg1	0.37	0.24	0.66
20	*YCL058C*	Fyv5	0.67	0.44	0.66
21	*YJL088W*	Arg3	0.37	0.25	0.68
22	*YDR448W*	Ada2	0.36	0.24	0.68
23	*YOL108C*	Ino4	0.47	0.32	0.69
24	*YOL095C*	Hmi1	1.22	0.84	0.69
25	*YDL077C*	Vam6	1.06	0.73	0.69
26	*YBR196C-A*	Ybr196c-a	0.40	0.28	0.69
27	*YDR017C*	Kcs1	0.82	0.57	0.69
28	*YBR282W*	Mrpl27	0.45	0.31	0.69
29	*YJR118C*	Ilm1	0.74	0.51	0.69
30	*YNL252C*	Mrpl17	0.28	0.20	0.69

SM, normalized colony size of single mutant; DM, normalized colony size of double mutant; DM/SM: colony size ratio of the double to single mutant.